JOURNAL OF PROPULSION AND POWER
Vol. 22, No. 3, May–June 2006

Electrospray Performance of Microfabricated Colloid Thruster Arrays

Matthew S. Alexander,* John Stark,† and Katharine L. Smith‡
University of London, London, England E1 4NS, United Kingdom
and
Bob Stevens§ and Barry Kent¶
Rutherford Appleton Laboratories, England OX11 0QX, United Kingdom

Microfabricated emitters have been produced by deep reactive ion etch technology. To demonstrate their suitability as components of integrated colloid thruster systems, we have evaluated the electrospray performance of individual and arrays of these microfabricated emitters and compared them to that of conventional stainless-steel emitters. We show that, after accounting for electrostatic differences caused by changes in physical geometry, the spray current dependence on flow rate for microemitters demonstrates similar scaling behavior to that of conventional single stainless-steel emitters. The spray current per nozzle is found to be independent of array size and the total spray current to depend simply on the number of nozzles in the emitter array. We have also found that in a triangular array of microemitters there is no significant geometry-induced shielding or field reduction between emitters. We report on the electrospray performance of the room- temperature ionic liquid 1-butyl-3-methylimidazolium tetrafluoroborate with conventional emitters, which appears to be a promising new colloid thruster propellant.

Nomenclature

a	=	power exponent
$f(\varepsilon)$	=	empirically derived parameter
I_n	=	spray current per emitter
I_{sp}	=	specific impulse
I_T	=	total spray current
Q	=	volumetric flow rate
Q_n	=	average flow rate throughput per nozzle
q/m	=	charge-to-mass ratio
T	=	thrust
γ	=	propellant surface tension
ΔP	=	differential pressure
ε	=	relative permittivity
ε_o	=	permittivity of vacuum
κ	=	propellant electrical conductivity
ρ	=	propellant density

I. Introduction

THE development of colloid thrusters for propulsive applications can be traced to the early 1960s (Refs. 1–3). They offer many desirable features when compared to other forms of propulsion, including high thrust density and high specific impulse at low power demand. Early work on the development of working colloid thrusters in the 1960s and 1970s suffered and generally failed however, principally as a result of poor technical understanding of the physical elements underlying the electrospray process, and hence control of critical parameters including the charge-to-mass ratio of sprayed droplets. Later, an improved understanding of electrospray processes followed from the work by Fenn's group at Yale[4] during the 1980s and from de la Mora's work[5] during the early 1990s. There is now a broad characterization of the relationship between stable flow rate, applied electric field, and the charge-to-mass ratio q/m of the electrosprayed charged droplets, although these relationships are principally derived from electrospray systems operating into a gas at atmospheric pressure.

This improved understanding has resulted in the recent development of a conventionally fabricated colloid thruster, consisting of 57 individual stainless-steel emitters brazed into a supporting structure,[6] which is designed to fly on space science missions such as LISA.

Highly doped organic solvents, such as formamide, and the high-conductivity room-temperature ionic liquids appear the most promising colloid propellants and are capable of providing specific impulse in excess of 500 s at modest acceleration voltages. The low thrust level delivered by a single electrospray emitter, typically in the order of only 0.1 μN, necessitates the use of large numbers of emitters if a sufficient level of thrust is to be obtained, to make such devices applicable to space missions. Space science missions such as LISA and LISA Pathfinder require thrust in the range 1–20 μN with a thrust noise level of below 0.1 μN, and for small satellites the thrust requirement is typically at the 1-mN level. Because of their compact size, colloid systems are very suitable for small satellites but these thrusters also have application in quite large coflying or station-keeping space missions such as XEUS and DARWIN. Reports on colloid thruster designs incorporating microfabricated emitter systems are limited. Workers at Massachusetts Institute of Technology (MIT)[7] have developed a microfabricated one-dimensional engine design consisting of a hydraulic system of fuel tanks, manifolds, and an array of 20 emitters fabricated in the silicon wafer plane. More recently the MIT group has produced a larger two-dimensional engine array of emitting elements that are externally wetted by the liquid under test.[8] They report the successful operation of these as electrospray sources in vacuum with the ionic liquid 1-ethyl-3-methylimidazolium tetrafluoroborate ($EmiBF_4$), although to avoid a buildup of insoluble or nonvolatile electrochemical products this type of array required operation in ac, rather than dc mode.

A joint development program between Queen Mary, University of London and Rutherford Appleton Laboratories has focused on the use of microfabrication techniques to produce multi-element

Received 19 December 2004; revision received 22 June 2005; accepted for publication 25 August 2005.

*Postdoctoral Research Assistant, Department of Engineering, Queen Mary.
†Head of Department, Department of Engineering, Queen Mary.
‡Ph.D. Student, Department of Engineering, Queen Mary.
§Process Technology Group Leader, Central Microstructure Facility.
¶Head of Applied Physics Group, Space Science and Technology Department.

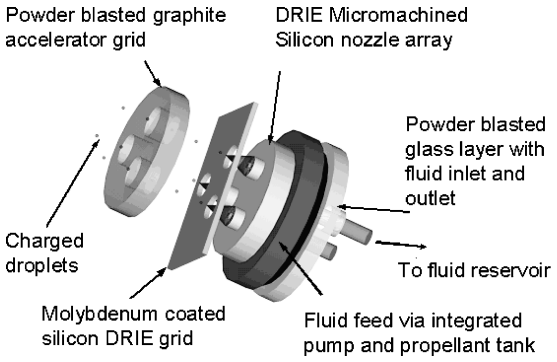

Fig. 1 Schematic of integrated colloid thruster system.

arrays of capillary emitters, with the end goal of developing a fully integrated colloid thruster, as illustrated in Fig. 1. A detailed description of the fabrication process is given elsewhere.[9] In this paper we report for the first time the performance of individual emitters and arrays of microfabricated silicon emitters, in which, unlike the early work on colloid thrusters in the 1960s, each emitter supports a single Taylor cone-jet structure. We compare here the electrospray properties of these microfabricated emitters with those sprays formed from conventional stainless-steel emitters and report their spray current flow-rate scaling behavior. We also report on the electrospray performance of the room-temperature ionic liquid 1-butyl-3-methylimidazolium tetrafluoroborate ($BmiBF_4$), which appears to be a promising new colloid thruster propellant.

II. Experimental Details

The fabrication procedure for the silicon microemitters, which involves deep reactive ion etch technology, is described in detail elsewhere.[9] This process can produce silicon nozzles with outer diameters from 560 to 35 μm, inner diameters from 305 to 25 μm and nozzle lengths of up to 400 μm. Triangular two-dimensional arrays of silicon microemitters on a hexagonal arrangement were produced with 3, 7, or 19 nozzles. Figure 2 shows an example of a 19 nozzle array after sputter coating with chromium and then a gold layer of 1–2 μm depth. The process is capable of producing extensive arrays and an example of a silicon wafer containing 20,000 nozzles within a 75-mm-diam area is shown in Fig. 3.

Previously reported work[9] tested these silicon nozzles after coating them with a chromium/copper layer of 1–2 μm thickness. This coating had been adopted to minimize wetting problems associated with the use of tri-ethylene glycol (TEG) doped with sodium-iodide (NaI) propellant selected for proof-of-concept electrospray testing. For all microemitter electrospray data in the current work, the emitters, were sputter coated with a gold surface layer of 1–2 μm thickness in order to provide improved corrosion resistance of the emitter.

A schematic of the electrospray test system is shown in Fig. 4. The stainless-steel capillaries used for comparison with the microemitters had an outer diameter of 560 μm, inside diameter of 305 μm, and were mounted in a standard SGE, Ltd., union to give a capillary length of 13 mm, an example of which is shown in Fig. 4b. The silicon microemitters were mounted in a specially designed steel and plastic holder as shown in Fig. 4d. The required electrostatic field at the emitter to achieve a stable Taylor cone-jet structure was obtained using a stainless-steel extractor electrode, which was fixed at an appropriate distance from the emitter, typically 3–4 mm. The extractor electrode had a 6-mm-diam centralized circular hole, which was optically aligned on the axis of the emitter. A flat-plate collector was positioned further 7 cm downstream from the extractor. The emitter/grid assembly was housed in a vacuum chamber, shown in Fig. 4: this was evacuated down to pressures below 10^{-3} mbar during testing using a turbomolecular pump backed by a rotary vane pump (RVP). The currents on the emitter and extractor electrode were measured online by a custom-built two-stage, optically isolated system.[10] This approach safely converted the signal

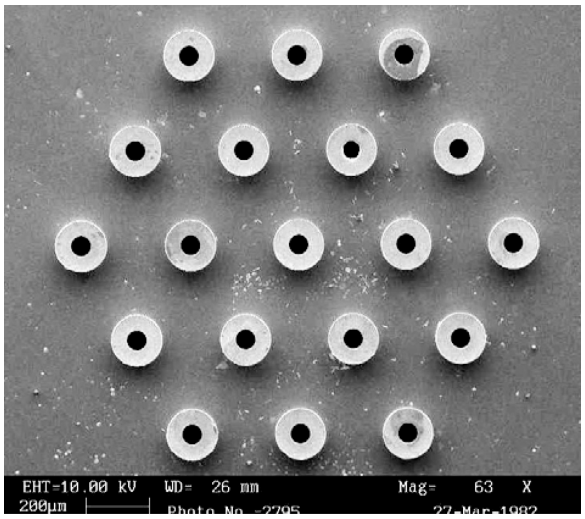

Fig. 2 Scanning-electron-microscopy micrograph of a microfabricated 19 emitter array.

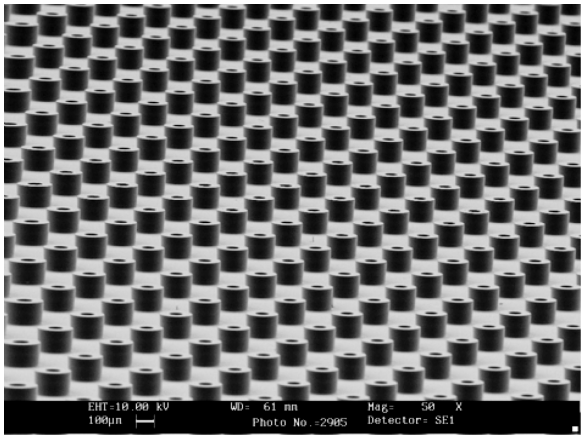

Fig. 3 Section of a microfabricated silicon wafer containing 20,000 nozzles in a 75-mm-diam area.

from high voltage to a data logger at ground potential. A battery-powered high-voltage stage, floated at the same potential as the emitter, contains a current-to-voltage converter in the transresistance configuration. This system was designed to measure currents up to ± 2 μA, with a voltage response of $\sim$1 mV/nA and a time response of 1 s. This converter is then followed by a voltage-to-frequency converter for optical signal transmission. A fiberoptic cable connected to a frequency-to-voltage converter chip at ground potential comprises the second stage, which is then directly and safely connected to a PC for data logging. Such isolation is clearly required on the high-voltage line to the emitter, but was also included on the extractor current monitor in order to protect instrumentation from a short circuit to high voltage. The current at the flat plate or Faraday cup collector was monitored using a Keithley Instruments picoammeter model 486, which was not interfaced to a data-logging computer.

A high-accuracy online flow-rate measurement system has been developed with an absolute volumetric flow-rate accuracy of $\sim$0.3 nL/s and a resolution of 0.03 nL/s. A full description of the instrument is provided in Ref. 11. This flow measurement is achieved by measuring the pressure drop between a pair of Paroscientific Digiquartz 740-23A quartz crystal pressure transducers. This pressure drop ΔP is directly proportional to the volumetric flow rate Q as described by the Poiseuille equation

$$Q = \Delta P \pi R^4 / 8 \mu L = \dot{m} / \rho \tag{1}$$

where $\dot{m}$ is the mass flow rate, ρ is the fluid density, μ is the fluid viscosity, R is the internal radius of the pipe section, and ΔP is

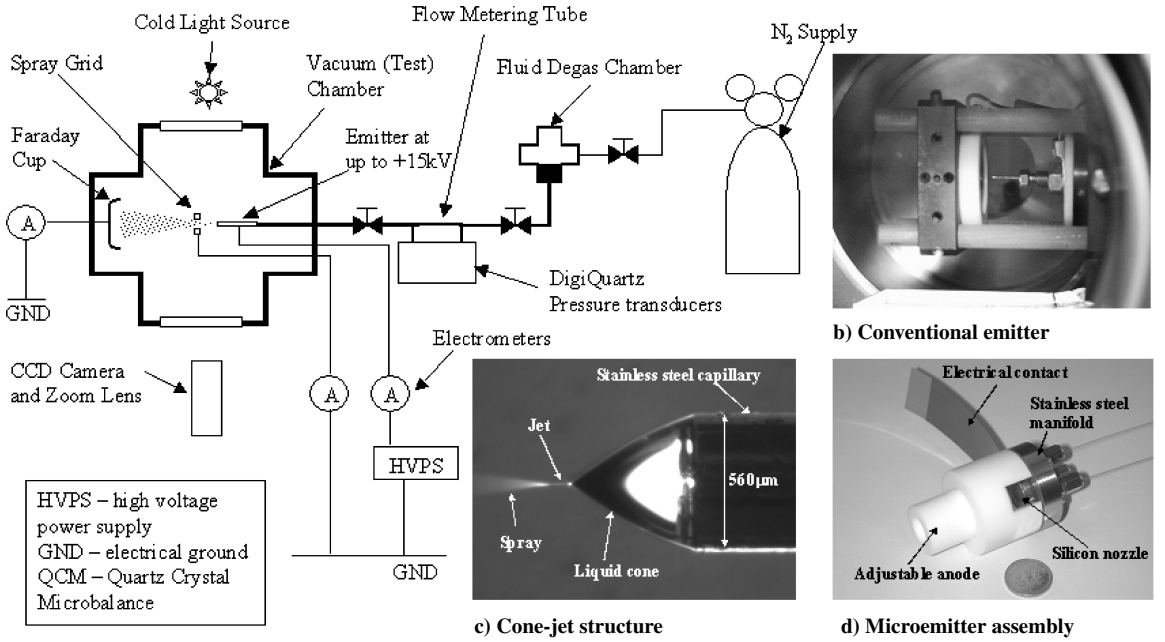

b) Conventional emitter

c) Cone-jet structure

d) Microemitter assembly

Fig. 4 Electrospray test rig configuration.

the pressure change along length L of the pipe. The pipe between the pressure transducers was a custom-made inert glass lined tubing GLT™ from SGE, Ltd. This was designed to minimize the use of unions and connectors in order to reduce both the dead volume of the system and the number of potential leakage sites for the ingress of air into the system. This pipework fitting consisted of a straight 150-mm-long measurement section with internal diameter of 0.3 mm and a tolerance of 0.29–0.33 mm. Two pressure tappings were located 25 mm from each end of the pipe section. These tappings, perpendicular to the flow bore, were 25 mm long and provided the interface with the pair of pressure transducers. The interface between the transducers and the test fluid is via a short section of transparent plastic pipe filled with a buffer fluid of silicone oil (Dow Corning FS1265). The buffer protects the transducer heads from chemical attack by the test fluids. Before use of a new liquid, the immiscibility of the new fluid and the silicone oil buffer was determined by long-term mixing tests and subsequent examination by Fourier transform infrared of each fluid layer, to confirm the absence of cross contamination. To obtain accurate flow data, it is essential to ensure that the interface between the test fluid and the buffer oil is gas free. This required the evacuation of the tubing to below $\sim 5 \times 10^{-3}$ mbar using a RVP to remove air from the system prior to the filling of the tubing with working fluid. The fluid was then fed into the tubing from the reservoir so that an air-free liquid-liquid interface between the silicone oil and the test fluid was formed. The system was calibrated by collecting a fluid sample at a fixed flow rate over a specific time period while recording the differential pressure between the two transducers ΔP. The collected sample was then weighed and the volumetric flow rate determined from the measured mass flow rate and the fluid density, as in Eq. (1). With hygroscopic fluids such as TEG, it was necessary to collect the sample under a dry nitrogen atmosphere to minimize water absorption from the air prior to weighing of the calibration sample. This procedure was repeated at a range of flow rates to determine the linear dependence of ΔP on the volumetric flow rate Q for the fluid under test. An example calibration plot for TEG + 12.5g/L NaI ($\kappa = 0.01$ S/m) is shown in Fig. 5. The electrospray measurements were obtained with the microemitter having high positive applied voltage, which required the isolation of the pressure transducers from ground potential.

The cone-jet structure of the electrospray was visualized, through a view port in the main vacuum chamber, using a PULNiX TM-1300 monochrome charge-coupled-device (CCD) camera in conjunction with a Navitar 12:1 telescopic zoom lens. The overall horizontal

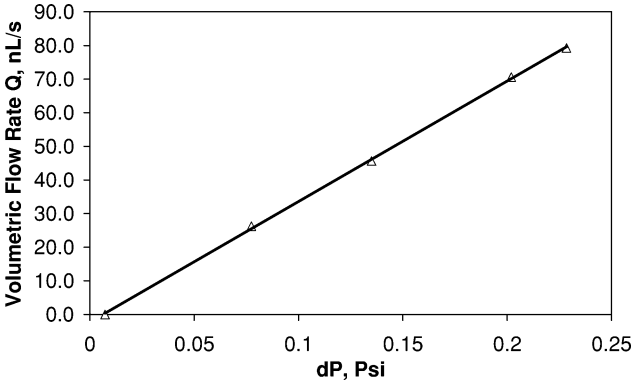

Fig. 5 Example flow-rate calibration curve for TEG + 12.5 g/L NaI ($\kappa = 0.01$ S/m).

and vertical resolution of the imaging system is 5 μm. This imaging system was used to determine if the electrospray were operating in stable cone-jet mode, as illustrated in Fig. 4c, and that there was no observable corona.

The TEG and NaI used in our experiments were purchased from Sigma-Aldrich, and the ionic liquid $BmiBF_4$ was obtained from Solvent Innovation GmbH (Koln, Germany). The conductivity and permittivity of the solutions used in our tests were determined using a novel triangular waveform method, which is described in Ref. 12.

III. Electrospray Results

A. Tri-Ethylene Glycol Solutions Doped with NaI

The effect of applied voltage on the spray current for conventional steel emitters with doped TEG propellant at differing fixed flow rates is shown in Fig. 6. The spray current appears largely independent of test voltage at the lowest flow rates tested, but exhibits a higher sensitivity to voltage as the flow rate is increased. It can also be observed from Fig. 6 that as the flow rate increases the onset voltage for stable cone-jet operation also increases. Stable electrospray operation was observed with the microemitters, and the classical Taylor cone-jet and spray structure was observed, as shown in Fig. 7b. Images of the cone-jet structure from the stainless steel and the microemitter at onset voltage are shown in Figs. 7a and 7b, respectively. One clear difference in the shape of the cone-jet structures is the greater elongation observed in the cone structure formed in the microemitter

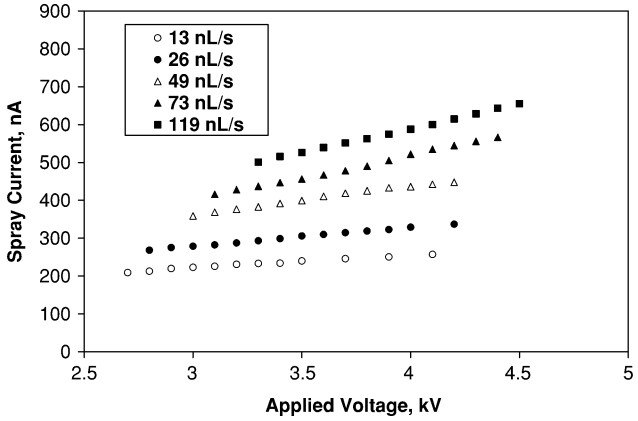

Fig. 6 Electrospray stability map for TEG + 12.5 g/L NaI (κ = 0.01 S/m) with conventional steel emitter.

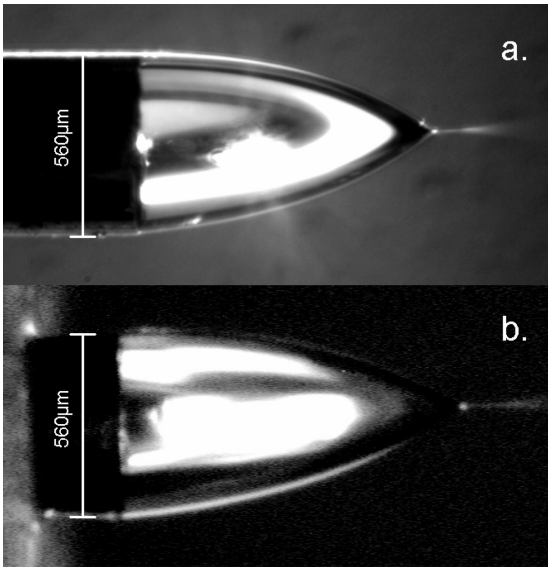

Fig. 7 Cone shape comparison between microemitter and steel capillary.

configuration. The data presented in Fig. 8 show the spray current dependence on the applied voltage for a conventional stainless-steel capillary and a microfabricated silicon microemitter at similar flow rates. The spray data were obtained from a steel capillary and a gold coated microemitter with identical outer and inner diameter values of 560 and 305 μm, respectively. The capillary length was 13 mm, whereas the microemitter had a height of only 400 μm above the surrounding surface. With the conventional emitter a sharp increase in spray current was observed at 4.6 kV. This higher current was caused by the transition from single cone-jet mode to multijet electrospray mode. The multijet spraying mode was not observed in the microemitter configuration over the voltage range tested. Instead of multijet mode, as the test voltage was increased the spray current became more sensitive to applied voltage but continued to operate in single cone-jet mode. As expected, the onset voltage for stable cone-jet operation is significantly higher for the microemitter compared to the stainless-steel capillary. This effect is because of the different physical geometries of the emitters tested. The field strength at the emitter tip region is defined by the emitter geometry, and the lower aspect ratio of the microemitter leads to a lower field strength at the emitter tip at equivalent applied voltages when compared to the stainless-steel capillary. Further evaluation of the field strength dependence for these two configurations is given in Ref. 9.

By assuming that at the onset voltage, when the first stable cone-jet spray is formed at a particular flow rate, the field strength at the cone apex will have a similar magnitude regardless of the emitter

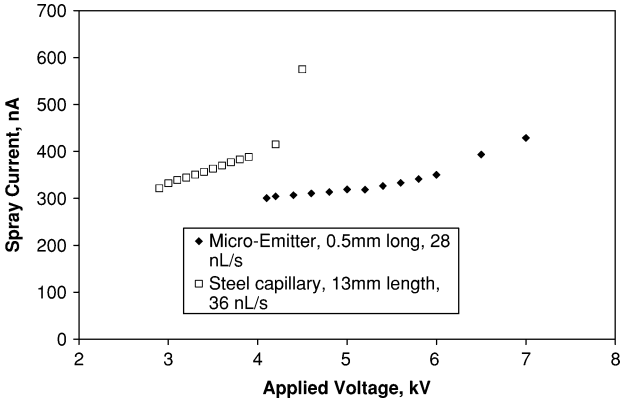

Fig. 8 Comparison of spray current voltage behavior for steel capillary and a single microemitter.

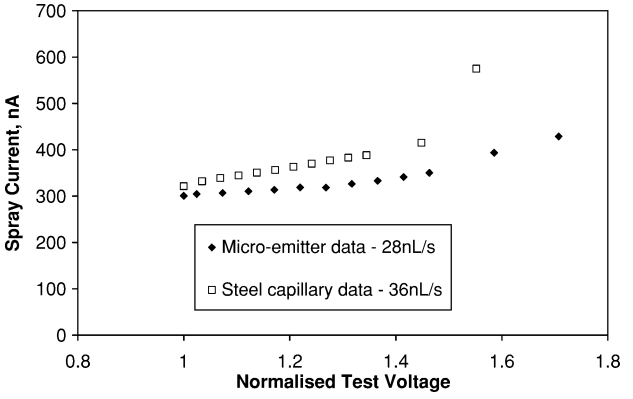

Fig. 9 Spray current against normalized voltage for steel capillary and single microemitter.

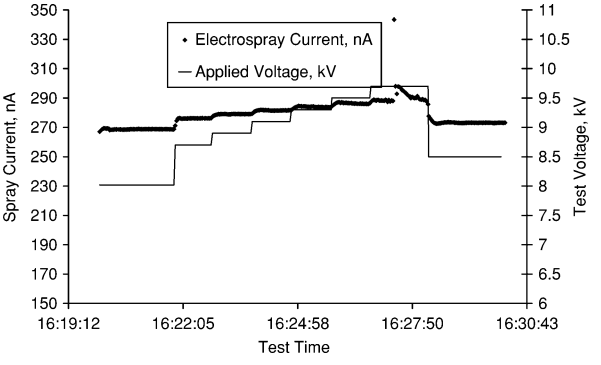

Fig. 10 Variation in spray current and applied voltage with time using single microemitter and flow rate of 18.5 nL/s.

geometry, then this voltage can be utilized to normalize the spray data from different emitter geometries and emitter/grid spacing. By normalizing the spray data by onset voltage in this way as shown in Fig. 9, it can be seen that the operating range of the stable cone-jet mode is essentially the same for the conventional stainless-steel emitter and the microfabricated microemitter, but without the occurrence of a sharp transition to multijet spray mode with the microemitter configuration.

The data shown in Fig. 10 were from a single microemitter with a smaller outer diameter of 178 μm, inner diameter of 50 μm, a height of 400 μm, and an emitter-to-extractor grid spacing of 4 mm. The plot shows continuous spray data from a 10-min test period during which the voltage was varied from the onset voltage of 8.02 to 9.5 kV, where a periodic instability in the spray current was measured. No multijet mode was observed in the microemitter configuration. Testing at significantly higher voltages than 9.5 kV was hindered by the

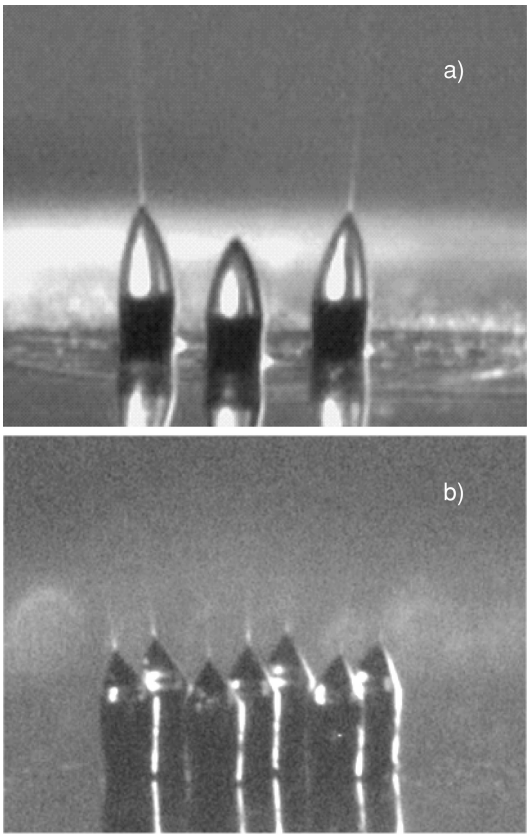

Fig. 11 CCD images of cone-jet structures formed on a microfabricated a) three emitter array and b) seven emitter array.

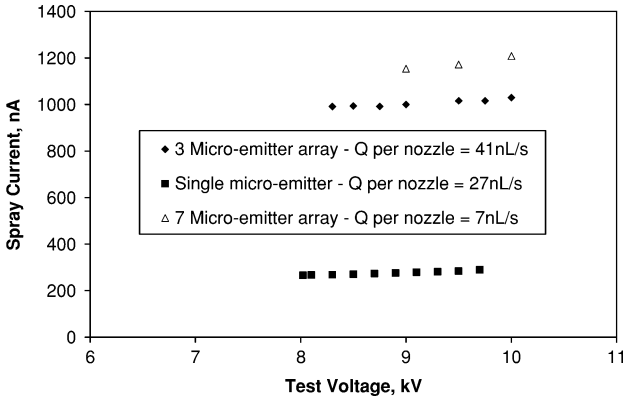

Fig. 12 Comparison of spray data for 1, 3, and 7 nozzle microemitters with TEG (0.01 S/m) propellant.

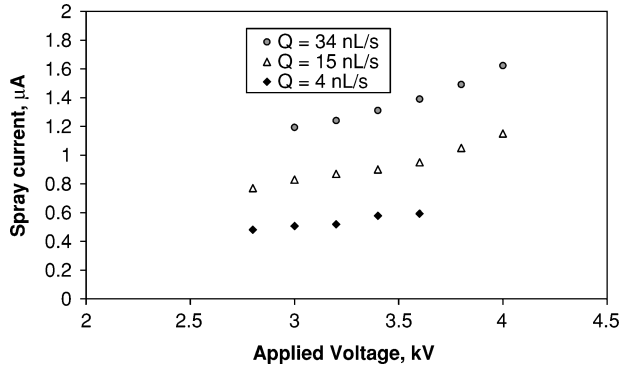

Fig. 13 Spray current dependence on voltage for $BmimBF_4$ with conventional emitter.

onset of electrical discharge between the emitter and grid electrode. Such discharge clearly acts to reduce the field strength and hence suppresses stable multijet mode. Instead we believe that the instability noticed as the voltage is increased is caused by an attempt to progress to multijet and hence the higher current noted, followed by discharge, which suppresses the stable transition to multijet mode. The bulk chamber pressure during testing, typically below 10^{-4} mbar, should prevent electrical discharges from occurring. However, the local pressure in the cone-jet region can increase because of the presence of electrosprayed droplets and solvent evaporation, leading to electrical discharge.

Stable electrospray operation of microfabricated arrays was observed with the TEG propellant, where each emitter supported a single Taylor cone-jet structure, as shown in Figs. 11a and 11b. The spray current voltage behavior for arrays of 3, 7, and an individual microemitter, all with outer diameter of 178 μm, inner diameter of 50 μm, and height of 400 μm is shown in Fig. 12. The pitch of both the three and seven emitter arrays tested was 175 μm. The value of onset voltage for stable cone-jet operation with the individual microemitter and the three emitter array show similar values. The slightly higher onset voltage with the three array is expected because of the higher flow rate through each nozzle of 41 nL/s compared with 27-nL/s flow rate through the individual emitter. This indicates that there is no significant electrical shielding or reduction in field strength as a result of the geometry of the triangular three emitter array. However, despite a lower flow throughput per nozzle of 7 nL/s in the data from the seven emitter array a substantially higher onset voltage was required for stable cone-jet spraying. During testing, it was noted that the central conejet was the first to show destabilization and cone-tip oscillation on lowering the voltage. This cone also appeared to be more elongated than the outer cone jets during spraying. This suggests that, in this configuration in which a single extraction electrode is used for multiple emitters, electrical shielding by the outer nozzles leads to a lower field strength on the central emitter, which leads to the higher onset voltage. Other workers who have studied the spray behavior and stable voltage regime of conventional emitters assembled into arrays have noted a similar trend of higher operating voltage with increasing sized arrays because of electrical shielding. Rulison and Flagan[13] studied a linear array of six conventional capillaries and observed an increased onset voltage and lower field strength on emitters in the middle of the array. Regele et al.[14] tested a two-dimensional array of four conventional capillaries and found that the potential required for stable cone-jet operation was higher and generally increased as capillary spacing decreased.

Apart from the higher voltage requirement of the seven emitter array, the spray current voltage behavior for the microfabricated emitters showed a slight sensitivity to voltage over the stable spray range, which was typical of conventional emitter behavior with TEG.

B. Ionic Liquid $BmimBF_4$ Propellant

The recently discovered room-temperature ionic liquids based on the imidazolium salts appear ideally suited for use as colloidal thruster propellants because of their high conductivity in the pure state and their negligible vapor pressure. A number of studies on the electrospray behavior of these ionic liquids has been reported. Gamaro-Castano[15] studied the electrospray performance of 1-ethyl-3-methylimidazolium bis(trifluoromethylsulfonyl) imide (EmiIm) propellant using a conventional six emitter array, and workers at MIT[8] have successfully operated a microfabricated colloid thruster device using the ionic liquid $EmiBF_4$ as propellant.We have tested the electrospray performance of the ionic liquid $BmiBF_4$ with conventional steel emitters, and the dependence of spray current on voltage at several flow rates is shown in Fig. 13. Stable cone-jet spraying was observed over a similar voltage range to that of TEG solutions with occurrence of multijet spraying mode at higher applied voltages. At fixed flow rate, the spray current showed a slight sensitivity to voltage over the stable cone-jet regime and generally increased as the extractor voltage was increased, in a similar way to the behavior observed for the conventional TEG solution. The

sensitivity of the spray current to voltage appeared to increase as the nominal flow rate was increased.

IV. Current Scaling Behavior

Scaling laws for the spray current emitted from conventional emitters in the cone-jet mode have been reported by several workers. Fernandez de la Mora and Loscertales[5] developed an empirical model using high-conductivity, high-permittivity fluids and reported the relationship

$$I = f(\varepsilon)\{Q\kappa\gamma/\varepsilon\}^{0.5} \tag{2}$$

where γ is the fluid surface tension and κ is the conductivity. This relationship can be represented by the general form

$$I = \text{const.}\,Q^{a} \tag{3}$$

A later study by Ganan Calvo et al.[16] identified two distinct regimes for the spray current flow rate dependence. The scaling behavior was found to depend strongly on the physical properties of conductivity and viscosity in such a way that with high-conductivity, high-viscosity fluids the current followed a power-law relationship as shown in Eq. (3) with an exponent value of 0.5; however, when fluids with low conductivity and low viscosity were studied the current scaling exhibited a power-law relationship with exponent value 0.25. Given the conductivity and viscosity parameters for the fluids used in our work, the appropriate exponent a, based on Ganan-Calvo's model, is however still a value of 0.5, and the overall current scaling behavior would be

$$I/I_o = 6.2\left[Q\Big/Q_o.(\varepsilon-1)^{0.5}\right]^{0.5} - 2 \tag{4}$$

where $I_o = (\varepsilon_o\gamma^2/\rho)^{1/2}$, $Q_o = (\gamma\varepsilon_o/\rho\kappa)$, and ε_o is the permittivity of a vacuum. Neither study reported in Refs. 5 and 16 indicated any significant dependence of the spray current behavior on applied voltage, although recently reported data from Ku and Kim[17] on the electrospray properties of glycerol solutions into vacuum suggest a sensitivity of spray current on operating voltage.

A. Current Scaling of Conventional Emitters

The spray current flow-rate behavior of conventional single emitters with doped TEG as propellant is shown in Fig. 14. The best-fit trend line for the data indicates that the spray current flow rate relationship is of a power-law dependence as in Eq. (3); however, the exponent value is 0.36. This exponent value is significantly different to the 0.5 value predicted in the work of Fernandez de la Mora and Loscertales[5] and Ganan-Calvo et al.[16] One noteworthy difference with the present work is that our electrospray tests are performed in a vacuum rather than atmospheric pressure as with the work in Refs. 5 and 16.

From the scaling data for $BmiBF_4$ in Fig. 15, the spray current follows a similar relationship to that of the TEG solution previously

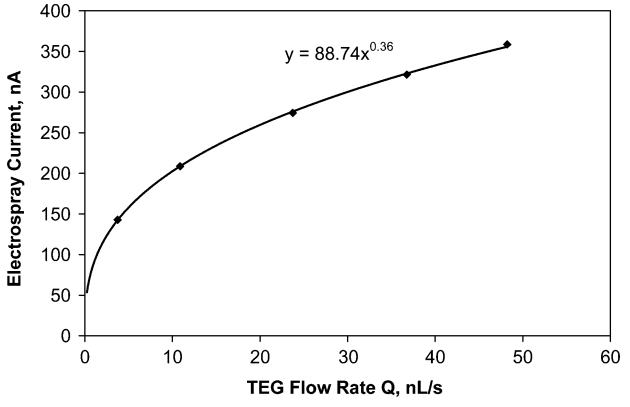

Fig. 14 Spray current flow-rate behavior of TEG ($\kappa = 0.01$ S/m) with conventional emitters.

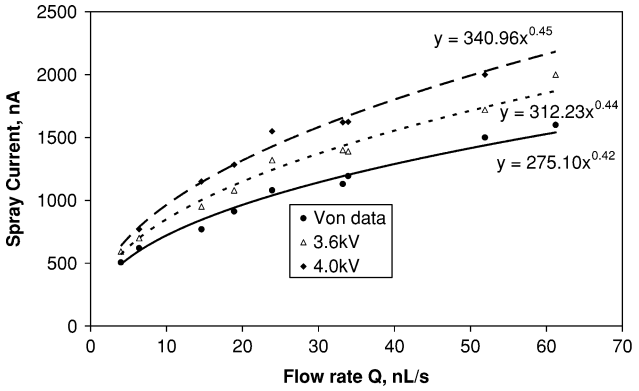

Fig. 15 Spray current flow-rate behavior of $BmimBF_4$ with conventional emitters.

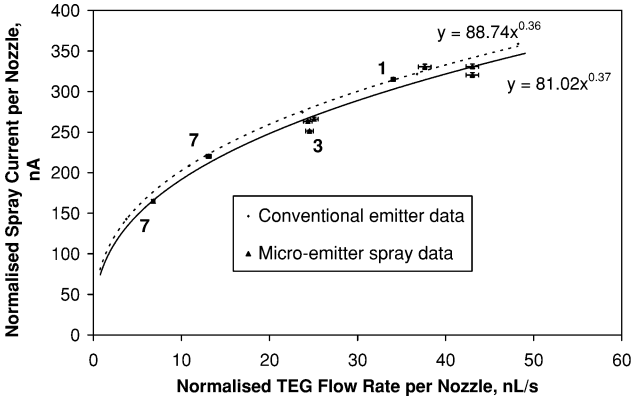

Fig. 16 Normalized spray current flow rate data for microemitter arrays with TEG ($\kappa = 0.01$ S/m) at onset voltage.

tested and of the same form as described in Refs. 5 and 16. However, it appears that the spray current flow-rate dependence is sensitive to the electrostatic test conditions with the power fit exponent value increasing from 0.42 at onset voltage to 0.45 at 4 kV. This behavior is not reported for electrospray testing at atmospheric pressure[5,16] and can only be observed under vacuum electrospray conditions. To give a more precise and reproducible current scaling relationship for the $BmiBF_4$ fluid tested, the data at onset voltage only will be considered for further discussion of the results. For the data at onset voltage, the best-fit power exponent a was found to be 0.42, which is closer to the 0.5 value predicted by the work in Refs. 5 and 16 but is still markedly different to the established scaling laws. The scaling-law exponent value of 0.42 is higher than the value of 0.36 found for the conventional organic solvent/salt solution of TEG + NaI described above.

B. Current Scaling of Microemitters

As discussed earlier, the stable operating voltage regime with microemitters is significantly higher when compared to conventional emitters caused by geometry effects and electrical shielding from adjacent nozzles in larger arrays, with a single extractor electrode. To overcome differences in field strength and to allow comparison with spray data from conventional single emitters, the spray current flow rate curves were constructed from data obtained at onset voltage for each flow rate only. The spray current data from arrays of microemitters were then normalized by dividing both the spray current and total flow rate by the number of nozzles in order to identify the spray current per nozzle I_n data for the arrays of microemitters. The normalized spray current flow rate data from microfabricated emitters with 1, 3, and 7 nozzles are plotted in Fig. 16, with the best-fit trend line for the conventional emitters from Fig. 14 also shown for comparison. The size of the array corresponding to each data point on the curve is also shown. The performance of the microemitters is

very similar to the conventional emitter data, with a best-fit power exponent value of 0.37, compared to 0.36 for the conventional emitter data. These data indicate the electrospray performance of the microemitters is comparable to that of conventional steel capillaries with the spray current dependent on flow rate and independent of emitter geometry and size of array. The observations demonstrate the important result that the total spray current from arrays of microemitters is indeed simply a function of the number of emitters, where the total spray current $I_T = nI_n$ and $I_n = \text{const.}\, Q_n^a$, where Q_n is the average flow rate through each nozzle.

V. Spray Current Stability

A. Triethylene Glycol Doped with NaI

For colloid thrusters to be suitable for space missions, such as LISA, an overriding requirement is for a low-thrust noise level. For example, in the LISA mission the thrust noise requirement is below the 0.1-μN level in the measurement frequency band of 0.1 to 100 mHz. The actual thrust level produced from the electrospray beam was not directly measured in the present work. However, if a steady thrust level is to be achieved from a colloid thruster then a stable spray current is a necessary requirement of that system. Real-time spray current data for a single microemitter with TEG (0.01S/m) over 10-min test period, along with the online flow-rate data for comparison, are shown in Fig. 17. The sampling rate for the data is one sample per second, and the standard deviation in the spray current data over the 10-min period in only 0.39% of the mean current value of 329nA. A potential source of noise in the electrospray current is from variations in the voltage applied between the emitter and grid. Our high-voltage power supply, a model HCL 14-20000 from F.u.G. Electronik GmbH, has a typical residual ripple of 5×10 pp or $\sim$0.005% of applied voltage. Although the output voltage during testing was not measured, the predicted low level of voltage noise, combined with the low sensitivity of the spray current to voltage, means that the effects of any voltage fluctuations on the spray current in the present work will be small and can be ignored.

The data presented in Fig. 18 compare the spray current stability of a single microemitter with the stability of a seven-microemitter array. The spray current data for the array have been normalized to give the spray current per microemitter I_n for clearer comparison. These data reveal that there is now a slightly higher spray current noise value of 0.92% of the mean 220-nA per microemitter value over the period tested. This higher noise might be caused by the nonuniformity in the field strength experienced by microemitters in the seven emitter array as a result of the geometry of the extractor grid. We anticipate this effect can be reduced by giving better consideration to extractor grid design, to incorporate individual apertures aligned above each microemitter, unlike the single large-aperture grid electrode used in the current work. Using the spray current data in Fig. 18, we can calculate the average charge-to-mass ratio q/m of the emitted charged droplets in the electrospray from

$$q/m = I/Q\rho \tag{5}$$

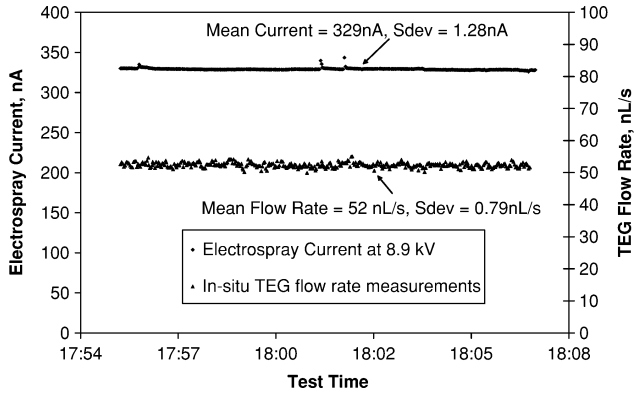

Fig. 17 Spray current and flow-rate stability for single microemitter with TEG (0.01 S/m) propellant.

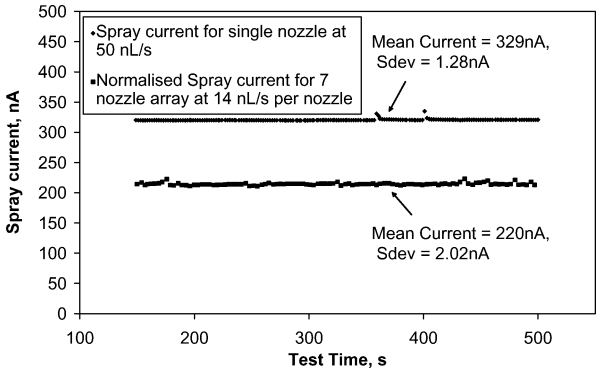

Fig. 18 Comparison of spray current stability for single nozzle and seven nozzle microemitters.

The expected thrust T produced from electrosprayed droplets is also dependent on the net acceleration voltage V and is

$$T = \rho Q(2V.q/m)^{0.5} \tag{6}$$

The spray data from the seven nozzle array at a flow rate per nozzle Q_n of 13.7 nL/s gives a q/m of $\sim$14 C/Kg and a thrust, assuming a modest acceleration voltage of 2 kV, of 3.7 $\pm$0.017 μN (or 0.46%) per nozzle. Therefore, the thrust delivered by the seven emitter array, at the flow rate per nozzle Q_n of 13.7 nL/s, is 25.9 μN $\pm$0.12 μN, which is above the higher level of thrust required by the LISA mission for example. By scaling to the upper level of thrust required for the LISA mission of 20 μN and assuming proportional thrust noise of 0.46%, this system would deliver 20 $\pm$0.092 μN, which is within the thrust noise limits of the mission. However, the modest conductivity of 0.01 S/m makes the TEG solution unsuitable for use as a colloid thruster propellant for space science mission applications because of its low q/m and hence low value of specific impulse I_{sp}.

B. BmimBF$_4$ Propellant

With a conductivity of 0.28 S/m, the ionic liquid BmiBF$_4$ is far more suitable as a colloid thruster propellant. The I_{sp} and thrust at any flow rate can be predicted by the empirical current scaling relationship found in the current work to be

$$I = 275.1Q^{0.42} \tag{7}$$

where the spray current is in nanoamperes and the flow rate of propellant Q in nanoliters/second. The I_{sp} increases as flow rate decreases and will be highest close to the minimum stable flow rate Q_{min}. Using the expression derived by Fernandez de la Mora and Loscertales[5] for the minimum flow rate

$$Q_{min} = \gamma\varepsilon\varepsilon_o/\rho\kappa \tag{8}$$

Using our measured properties for liquid conductivity, permittivity, and surface tension, the value of Q_{min} for the ionic liquid BmiBF$_4$ is predicted to be 7.75×10^{-14} m^3/s. This flow rate is below the detection limit of our current flow-rate measurement system. However if we were to interpolate using Eq. (7), we can derive a minimum spray current value I_{min} to be 94 nA. Assuming a 20-kV acceleration voltage, the specific impulse at Q_{min} for the BmiBF$_4$ propellant would be 663 s, which is above the 500 s required for the propulsion system to become competitive relative to other propulsion options for typical space science mission applications.[18] This I_{sp} value is significantly improved over bipropellant systems with a typical I_{sp} of $\sim$350 s. Considering the LISA mission itself, several alternative propulsion methods have been proposed including a cold-gas microthruster[19] and a field effect electric propulsion (FEEPs)[20] system. Evidently the I_{sp} from the BmiBF$_4$ colloid thruster is much improved over the cold-gas system, whose I_{sp} is in the range 60 to 80 s, but offers lower performance when compared to the FEEPs system, being typically around 5000 s. The variation in thrust and

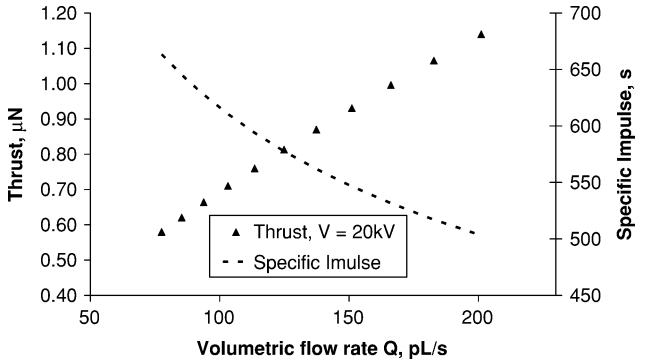

Fig. 19 Effect of $BmimBF_4$ flow rate on specific impulse and thrust for a single emitter.

I_{sp} with increasing flow rate for a single $BmiBF_4$ colloid emitter is shown in Fig. 19. This demonstrates one attractive feature of colloid thrusters in that the thrust can be varied in a number of ways. These include variation of the propellant mass flow rate, of the applied acceleration voltage, and by operation of discrete areas of differing size arrays, as described more fully in Ref. 21. This allows a large variation in the trust achievable with a colloid system and gives added flexibility to realize a thrust solution closer to the optimum. With a minimum I_{sp} requirement of 500 s, the maximum flow rate throughput of $BmiBF_4$ propellant allowable for each emitter is $\sim$0.2 nL/s, at which the thrust from a single microemitter would be 0.58 μN (at 20-kV acceleration voltage) as shown in Fig. 19. This demonstrates that the upper operational thrust level of 20 μN for the LISA mission is achievable with an array size of 35 microemitters. Assuming a similar nozzle density as the microfabricated wafer shown in Fig. 3, the 35 emitter array could be fabricated out of a circular wafer with diameter of 3.1 mm. For the 100-μN thrust per head requirement for the SNAP-2 mission, discussed in Ref. 21, an array size in the order of 175 microemitters will be required, which could be produced within a circular diameter of only 7 mm.

VI. Conclusions

We have produced a range of microfabricated emitters and evaluated their electrospray performance. Comparison of spray properties from microemitters and conventional steel emitters has identified that the cone structure is different at similar flow rates, with a longer Taylor cone in the case of the microemitters. This is principally associated with the different field structure around the shorter microemitters relative to the longer steel capillaries used in our experiments.

The spray current flow-rate scaling behavior of both the conventional doped organic solvent and the ionic liquid propellants tested were found to fit a power-law relationship. The power-law exponent values were determined to be 0.36 and 0.42 at onset voltage for the TEG and $BmiBF_4$ propellants, respectively. The power-law exponent was found to be sensitive to the applied voltage, with an increasing exponent value at higher test voltages.

Good electrospray current stability was observed with current noise levels of below 0.5% of the mean spray current with single nozzles, which increased to 0.92% with larger arrays. We anticipate a reduction in spray current noise will be achieved by our next generation of microemitters with integrated microfabricated extractor grid structures with individual apertures positioned above each nozzle. This is predicted to give improved uniformity in the field strength experienced by each element of an array and give higher spray current and thrust stability.

The ionic liquid $BmiBF_4$ was shown to be a promising colloid thruster propellant capable of achieving a specific impulse in excess of 500 s near minimum flow rate. It was shown to operate in stable cone-jet mode with emission of positively charged droplets and to exhibit a transition to multijet spraying mode on increasing extractor voltage.

Acknowledgments

This research project was supported by Engineering and Physical Sciences Research Council Grants GR/R21936 & GR/R21943.

References

[1]Bailey, A. G., *Electrostatic Spraying of Liquids*, Research Studies Press, Ltd., Taunton, Somerset, England, UK, 1988, Chap. 8, pp. 171–176.

[2]Hendricks, C. D., "Charged Droplet Experiments," *Journal of Colloid and Interface Science*, Vol. 17, No. 3, 1962, pp. 249–259.

[3]Perel, J., Bates, T., Mahoney, J., Moore, R. D., and Yahiku, A. Y., "Research on a Charged Particle Bipolar Thrustor," AIAA Paper 67-728, 1967.

[4]Fenn, J. B., Mann, M., Meng, C. K., Wang, S. K., and Whitehouse, C., "Electrospray Ionization for Mass-Spectrometery of Large Biomolecules," *Science*, Vol. 246, No. 4926, 1989, pp. 64–71.

[5]Fernandez de la Mora, J., and Loscertales, J. G., "The Current Emitted by Highly Conducting Taylor Cones," *Journal of Fluid Mechanics*, Vol. 260, 1994, pp. 155–184.

[6]Hruby, V., Gamero-Castono, M., Falkos, P., and Shenoy, S., "Micro Newton Colloid Thruster System Development," IEPC-01-281, ERPS, Cleveland, OH, 2001.

[7]Velasquez, L. F., and Marinez-Sanchez, M., "A Micro-Fabricated Colloid Thruster Array," AIAA Paper 2002-3810, July 2002.

[8]Velasquez, L. F., Carretero, J. A., Ankinwande, A. I., and Martinez-Sanchez, M., "The Concept and Development of a Micro-Fabricated Colloid Thruster Array," AIAA Paper 2003-4850, July 2003.

[9]Stark, J., Stevens, B., Alexander, M., and Kent, B., "Fabrication and Operation of Micro-Fabricated Emitters as Components for a Colloid Thrusters," *Journal of Spacecraft and Rockets*, Vol. 42, No. 4, 2005, pp. 628–639.

[10]Aplin, K., "Opto-Isolated Current Measurement System," Rutherford Appleton Labs., Space Science and Technology Div. Rept., Oxfordshire, England, UK, July 2002.

[11]Smith, K. L., "Characterisation of Electrospray Properties in High Vacuum: with a View to Application in Colloid Thrusters Technology," Ph.D. Dissertation, Dept. of Engineering, Queen Mary, Univ. of London, UK, May 2005.

[12]Wu, J., and Stark, J. P. W., "A Low-Cost Approach for Measuring Electrical Conductivity and Permittivity of Liquids by Triangular Waveform Voltage," *Measurement Science and Technology*, Vol. 16, No. 5, 2005, pp. 1234–1240.

[13]Rulison, A. J., and Flagan, R. C., "Scale-up of Electrospray Atomization Using Linear Arrays of Taylor Cones," *Review of Scientific Instrumentation*, Vol. 64, No. 3, 1993, pp. 683–686.

[14]Regele, J. D., Papac, M. J., Rickard, M. J. A., and Dunn-Rankin, D., "Effects of Capillary Spacing on EHD Spraying from an Array of Cone-Jets," *Journal of Aerosol Science*, Vol. 33, No. 11, 2002, pp. 1471–1479.

[15]Gamaro-Castano, M., "Characterisation of a Six-Emitter Colloid Thruster Using a Torsional Balance," *Journal of Propulsion and Power*, Vol. 20, No. 4, 2004, pp. 736–741.

[16]Ganan-Calvo, A. M., Davila, J., and Barrero, A., "Current and Droplet Size in the Electrospraying of Liquids-Scaling Laws," *Journal of Aerosol Science.*, Vol. 28, No. 2, 1997, pp. 249–275.

[17]Ku, B. K., and Kim, S. S., "Electrohydrodynamic Spraying Characteristics of Glycerol Solutions in Vacuum," *Journal of Electrostatics*, Vol. 57, No. 20, 2003, pp. 109–128.

[18]Stark, J., Paine, M., Kent, B., Stevens, B., Sandford, M., and Alexander, M., "Colloid Propulsion—A Re-Evaluation with an Integrated Design," AIAA Paper 2003-4847, July 2003.

[19]Nicolini, D., Ceruti, L., Kent, B., Santangelo, G., Serafni, L., and Solway, N., "MicroNewton Propulsion Developments for Drag-Free Spacecraft," ESA, Paper SP555, June 2004.

[20]Marcuccio, S., Giannelli, S., and Andrenucci, M., "Attitude and Orbit Control of Satellites and Constellations with FEEP Thrusters," IEPC, Paper 97-188, ERPS, Cleveland, OH, Aug. 1997.

[21]Kent, B., Stark, J., Stevens, B., Alexander, M., Baker, A., Gibbon, D., and Liddle, D., "A MEMS Based Experimental Colloid Thruster Package for Nano Satellites," AIAA/USU SSC04-X1-3, 2004.